PHYSICAL REVIEW B **77**, 075111 (2008)

Ab initio study of $SrFe_xTi_{1-x}O_3$: Jahn-Teller distortion and electronic structure

V. E. Alexandrov* and J. Maier
Max-Planck-Institut für Festkörperforschung, Heisenbergstrasse 1, D-70569 Stuttgart, Germany

R. A. Evarestov
Department of Quantum Chemistry, St. Petersburg State University, 26 Universitetskiy Prospekt, Stary Peterhof 198504, Russia

(Received 31 July 2007; published 12 February 2008)

We present and discuss first-principles calculations of the Jahn-Teller distortion and the electronic structure of the strontium titanate ferrite solid solution. It is shown that the use of the hybrid Hartree-Fock density functional theory approach with B3PW exchange-correlation functional enables a quantitative description of the experimentally found Jahn-Teller distortion in $SrFe_xTi_{1-x}O_3$. The results for various iron concentrations (50%, 6.25%, 3.70%, 3.125%, and 1.85%) corroborate very recent experimental findings.

DOI: 10.1103/PhysRevB.77.075111 PACS number(s): 71.15.Ap, 61.72.S−, 71.20.Be, 74.72.−h

I. INTRODUCTION

The technologically highly important ABO_3 perovskite compounds have been a subject of a huge number of experimental and theoretical studies during the past few decades. One driving force to study ABO_3 perovskites is the opportunity to control their electronic and ionic defect structures and, hence, to tailor those properties that determine a wide spectrum of applications (gas sensors, fuel cell cathodes, catalysis, substrates for growth of high-T_C materials, etc.). There is a large number of work devoted to first-principles studies of defective perovskites as to investigate atomic structure, electronic and magnetic properties, defect chemistry, etc.[1–3] Much of the reported studies have been based upon the density functional theory (DFT) formalism connected with plane-wave (PW) basis expansion. Defective $SrTiO_3$ is a very interesting material in this context as it is exhibiting both significant ionic and electronic conductivities due to the presence of mobile point defects (oxygen vacancies, excess electrons, and electronic holes).[4]

In particular, Fe-doped $SrTiO_3$ has attracted much experimental attention in view of studying atomic structure, defect chemistry, and transport properties.[5–7] The relation to the concentration of point defects has been thoroughly elucidated. The first *ab initio* study of Fe-doped $SrTiO_3$ has been performed in the framework of the unrestricted Hartree-Fock method in the linear combination of atomic orbitals approximation.[8] In that work a single iron impurity has been considered within the periodic supercell approach and a Jahn-Teller distortion has been predicted for the first time. A very recent experimental study[7] of the $SrFe_xTi_{1-x}O_3$ solid solution with well-defined oxygen stoichiometry by means of x-ray diffraction, x-ray absorption spectroscopy, and vibrational infrared and Raman spectroscopy has given clear evidence of the presence of a Jahn-Teller distortion around iron Fe^{4+} centers for low iron contents $x \to 0$. The mean square relative displacements (MSRDs) obtained from fitting the extended x-ray absorption fine structure (EXAFS) data, reflecting the distortion in the first oxygen shell, decrease monotonically for increasing iron contents. It should be noted that the Jahn-Teller distortion does not appear for the pure $SrFeO_3$.

In the present work we restrict our first-principles study to modeling the ideal composition $SrFe_xTi_{1-x}O_3$ with no oxygen vacancies present. First of all, we consider the two limiting cases of pure $SrTiO_3$ and $SrFeO_3$ to probe several computational schemes on a number of bulk quantities and band structure calculations. As the primary approach we choose the hybrid HF-DFT methodology with B3PW functional[10] which results in very good agreement with experimental data on structural and energetic properties including band gap. Moreover, within the linear combination of atomic orbitals (LCAO) approximation, a hybrid method also permits one to analyze crystalline orbitals as well as different properties of a system in terms of atomic orbitals contributions which is more relevant from a chemical point of view.

One of the addressed questions is the accurate quantitative description of the Jahn-Teller distortion around iron Fe^{4+} centers for different iron contents in the $SrFe_xTi_{1-x}O_3$ solid solution which can be compared with the recent experimental data of Ref. 7. In addition, we explore the trends in changing the electronic structure for different levels of iron doping going from pure $SrTiO_3$ to pure $SrFeO_3$ and trying to compare the results with available experimental and theoretical data. For this purpose, we use both the plane wave and the LCAO approaches and exploit the different Hamiltonians in the LCAO method to critically analyze the obtained results.

The organization of this paper is as follows. Section II gives a brief overview of studies on the pure parent compounds of $SrTiO_3$ and $SrFeO_3$ as well as Fe-doped $SrTiO_3$. In Sec. III the used supercell model and computational details are discussed. Section IV deals with the calculation of bulk $SrTiO_3$ and $SrFeO_3$. The Jahn-Teller effect and electronic properties of $SrFe_xTi_{1-x}O_3$ solid solution are analyzed in Secs. V and VI, respectively.

II. PARENT COMPOUNDS ($SrTiO_3$ AND $SrFeO_3$) AND Fe-DOPED $SrTiO_3$: AN OVERVIEW

$SrTiO_3$ and $SrFeO_3$ perovskite crystals have been extensively studied both experimentally and theoretically over the past few decades. Both materials crystallize in exactly the same structure with $Pm\bar{3}m$ space group while exhibiting very different electronic properties. $SrTiO_3$ is a semiconductor with an experimental band gap of about 3.3 eV,[11] while

$SrFeO_3$ shows a metallic conductivity.[12] It is also well known from experimental data that these crystals do not exhibit a Jahn-Teller distortion.

A number of approaches have been applied to describe the properties of these systems. One of the useful semiempirical approaches is to use ligand field theory and cluster model calculations to interpret experimental spectra.[13] This approach allows one to qualitatively describe the electronic structure of a ground state by expanding it in terms of single ionic configurations which can significantly contribute to the ground state of a crystal. In Ref. 14 this approach has been applied to the interpretation of x-ray photoemission and ultraviolet photoemission spectroscopic data of $SrFeO_3$. It has been clearly shown that the simulation can reproduce the experimental spectrum only if several single configurations have been included in addition to the $d^4(t_{2g}^3 e_g^1)$ configuration. By using the configuration interaction (CI) cluster model with three adjustable parameters the authors have found that the ground state is dominated by the $3d^5\underline{L}$ rather than the $3d^4$ configuration (where $\underline{L}$ denotes a ligand hole) and that this can suppress the Jahn-Teller (JT) distortion of the d^4 ion. A large contribution of the $3d^5\underline{L}$ configuration to the ground state gives rise to the presence of itinerant d electrons, thus leading to metallic conductivity in $SrFeO_3$. This semiempirical model also enables one to discuss the effects of covalency by estimating the occupancies of different configurations. In Ref. 15, using the same approach for the interpretation of x-ray absorption spectra of $SrFeO_3$, the authors have obtained the following occupancies of different configurations in percentage terms: 36% $3d^4$, 58% $3d^5\underline{L}$, and 6% $3d^6\underline{L}^2$. The obtained population of the Fe $3d$ orbital is approximately 4.7 and hence larger than the pure ionic value of 4.0 reflecting the significant degree of covalency in $SrFeO_3$.

The electronic properties of $SrTiO_3$ and $SrFeO_3$ crystals have also been calculated by exploiting a number of *ab initio* approaches.[16–19] Band structure calculations of $SrTiO_3$ have confirmed the semiconducting nature of the crystal with the top of the valence band being predominantly formed by O $2p$ atomic orbitals and the bottom of the conduction band mainly consisting of Ti $3d$ states. The bond population analysis demonstrates a large overlap between O $2p$ and Ti $3d$ orbitals confirming the covalent nature of the Ti-O chemical bonding.[16] $SrFeO_3$ is much less understood. Its electronic and magnetic properties have been studied by means of the tight-binding linear muffin-tin orbital method within the atomic sphere approximation,[20] the augmented spherical wave method,[21] and pseudopotential LSDA+U (Ref. 22) band structure calculations. Also known are discrete variational method[23] calculations within the cluster model.[24] In Refs. 22 and 25 the ferromagnetic and different antiferromagnetic spin configurations of $SrFeO_3$ have been examined in DFT plane-wave simulations and the ferromagnetic state has been found to be the most favorable among the collinear magnetic phases. The energy bands, density of electronic states, and some bulk properties have been calculated. However, to the best of our knowledge, LCAO band structure calculations of $SrFeO_3$ have not been reported.

Owing to the very different properties of the end members it is of great significance to study the $SrFe_xTi_{1-x}O_3$. While these compositions have been experimentally investigated within quite an intensity even as a function of oxygen deficiency, there is still a lack of theoretical investigations. It is well known that in the perovskite cubic crystalline field the Fe $3d$ states split into t_{2g} and e_g levels. In the high-spin state with the total spin projection of $S=2$ three spin up electrons occupy the lower t_{2g} states while the upper e_g level is occupied by the fourth spin up electron. As shown in Refs. 8 and 26 there is an $E_g \otimes e_g$ Jahn-Teller distortion which gives rise to inward relaxation of four oxygen atoms in the xy plane near the iron defect and outward relaxation of two oxygen atoms along the z axis. Such a distortion yields further splitting of Fe $3d$ states according to the final symmetry.

In Ref. 8 the Jahn-Teller distortion in Fe-doped $SrTiO_3$ material has been theoretically predicted by applying the unrestricted Hartree-Fock (UHF) method within the supercell approach. For the case of a single iron impurity it has been found that four Fe–O bonds in the xy plane shorten by 0.028 Å (inward relaxation) and two Fe–O bonds along the z axis lengthen by 0.052 Å (outward relaxation) which yields an energy gain of about 1.42 eV with respect to the undistorted geometry. Also, it has been shown that the iron high-spin ($S=2$) state rather than the zero-spin ($S=0$) state is favored with an energy gain of about 5.4 eV.

The EXAFS study[7] mentioned above has permitted a quantitative estimate of the changes in Fe–O bond lengths for different iron concentrations in $SrFe_xTi_{1-x}O_3$ based upon the MSRD approximation.[9] A bond length distribution of 0.16 Å corresponding to a JT distortion has been assessed for the dilute limit and it has been also shown that some of the Fe–O bonds contract while the others expand. This experimental estimate can be compared with 0.08 Å, which is the sum of 0.052 Å elongation and 0.028 Å contraction obtained in the UHF method.[8] It is supposed that the UHF method underestimates the total magnitude of the oxygen displacements around the iron, nevertheless, giving the correct picture of the JT distortion and the related electronic structure changes.

In a very recent first-principles plane-wave DFT [local density approximation and generalized gradient approximation (GGA)] study[27] devoted to structural and electronic properties of Fe-doped $SrTiO_3$ and $BaTiO_3$ the JT distortion has not been taken into account in spite of the UHF prediction and the experimental evidence for Fe-doped $SrTiO_3$. As a result, the properties computed there, e.g., iron impurity formation energy, have certainly to be refined.

III. SUPERCELL MODEL AND COMPUTATIONAL DETAILS

In the present study of the $SrFe_xTi_{1-x}O_3$ solid solution we adopted a periodic supercell approach which is widely used in defective crystal calculations.[28] In such an approach an extended unit cell (supercell) is defined by a linear transformation connecting the basis translation vectors of the perfect crystal $\mathbf{a}_i$ with the translation vectors $\mathbf{A}_j$ of the supercell chosen as follows:

$$\mathbf{A}_j = \sum_{i=1}^{3} l_{ij}\mathbf{a}_i, |\det l| = L. \qquad (1)$$

In this work we considered supercells of different shapes and sizes by extending the initial lattice vectors of cubic $SrTiO_3$ and substituting the titanium atom in the origin of a cell by iron to create a defective system. The 135-atom simple cubic (sc), 80- and 270-atom face-centered cubic (fcc), and 160-atom body-centered cubic (bcc) cells were created by using the transformation matrices defined in Eq. (1),

$$\begin{vmatrix} n & 0 & 0 \\ 0 & n & 0 \\ 0 & 0 & n \end{vmatrix}, \quad \begin{vmatrix} 0 & n & n \\ n & 0 & n \\ n & n & 0 \end{vmatrix}, \quad \text{and} \quad \begin{vmatrix} -n & n & n \\ n & -n & n \\ n & n & -n \end{vmatrix}, \qquad (2)$$

respectively, where n is varied between 2 and 4.

The supercell with sc extension of $3\times3\times3$ contains 135 atoms and corresponds to 3.7% of iron concentration in $SrFe_xTi_{1-x}O_3$ solid solution. The supercells with fcc extensions of $\sqrt{2}\times\sqrt{2}\times\sqrt{2}$ (10 atoms), $2\sqrt{2}\times2\sqrt{2}\times2\sqrt{2}$ (80 atoms), and $3\sqrt{2}\times3\sqrt{2}\times3\sqrt{2}$ (270 atoms) are rhombohedral with an angle of 60° between the lattice vectors corresponding to 50%, 6.25%, and 1.85% of iron content, respectively. The last considered supercell is the 160-atom rhombohedral bcc cell with an angle of 109.47° (extension $2\sqrt{3}\times2\sqrt{3}\times2\sqrt{3}$) that corresponds to 3.125% of iron.

It is known[28,29] that both HF and DFT yield systematical errors with opposite sign with respect to the experiment whereas the formulation of hybrid functionals can improve the accuracy of the crystal calculations. This is the case for band gaps, phonon spectra, magnetic coupling constants, and all properties that depend upon the extent of electronic localization at either perfect, defect, or surface sites. Furthermore, it is well known that a hybrid HF-DFT method adequately reproduces the band gaps for insulators, whereas plain DFT methods underestimate this quantity considerably.[28] This point can be crucial when studying the defect level positions which often lie within the band gap. In addition, hybrid HF-DFT functionals usually allow one to reproduce the experimental lattice constants very well, thus being very efficient for the geometry optimization (see, e.g., the comparison of a large number of Hamiltonians for the calculation of $SrTiO_3$, $BaTiO_3$, and $PbTiO_3$ bulk properties in Ref. 16). In this context it should be noted that with existing computer codes the plane-wave simulations are possible only within the DFT formalism while the CRYSTAL-2006 LCAO code[30] allows one to exploit different Hamiltonians (Hartree-Fock, DFT, and hybrid HF-DFT). In a recent paper[31] it has been shown how the hybrid HF-DFT approach could be realized using a plane-wave basis set, but at the moment it is still unimplemented in the VASP code.[32,33] Owing to all these facts, we have chosen the hybrid HF-DFT methodology as the primary approach for the simulation of Jahn-Teller distortion and the electronic structure calculations. Nevertheless, to validate this method we compare it with other approaches and available experimental data.

In the present study we exploit the hybrid Hamiltonian in the LCAO basis with B3PW exchange-correlation functional[10] which includes the exchange part as the mixture of Fock (20%) and Becke's (80%) exchange while the correlation part is a Perdew-Wang nonlocal correlation functional. Also, we performed some of the calculations in the pure DFT-LCAO method with Perdew-Burke-Ernzerhof (PBE) functional[34] within GGA. Both hybrid HF-DFT and pure DFT LCAO calculations were carried out with the CRYSTAL-2006 computer code.[30] Small core Hay-Wadt pseudopotentials[35] are used for core electrons in the case of Sr and Ti atoms while the outermost shell basis functions were taken from the previous work[16] where these functions have been optimized for $SrTiO_3$ bulk crystal. For oxygen atoms all-electron Gaussian basis sets of type 8-411G* were taken from the same paper. The iron atom is represented on an all-electron basis from Ref. 36 where it has been optimized for the case of α-Fe_2O_3 (hematite). Our further optimization of this basis for bulk $SrFeO_3$ decreased the total energy insignificantly.

In all calculations we chose the thresholds of 10^{-6}, 10^{-6}, 10^{-6}, 10^{-6}, and 10^{-12} for the Coulomb overlap, Coulomb penetration, exchange overlap, the first exchange pseudo-overlap, and the second exchange pseudo-overlap, respectively. For the summation in the Brillouin zone (BZ) we adopted the Monkhorst-Pack[37] mesh of **k** points. In the cases of bulk $SrTiO_3$ and $SrFeO_3$ we studied the convergence of energy with increasing number of used **k** points in the BZ and found $8\times8\times8$ for the semiconductor $SrTiO_3$ and $16\times16\times16$ for the metallic $SrFeO_3$ to be large enough for achieving convergence.

In the geometry optimization process we reduced the symmetry of a supercell under consideration from cubic $Pm\bar{3}m$ to tetragonal $P4/mmm$ to be able to obtain Jahn-Teller distortion. In the CRYSTAL-2006 code atomic equilibrium positions are calculated by using the Schlegel conjugate gradient algorithm.[38] Convergence during the geometry optimization process is tested on the root mean square (rms) and the absolute value of the largest component of both the gradients and the nuclear displacements. The default thresholds for the maximum and the rms forces and the maximum and the rms atomic displacements on all atoms were set to 0.000 45, 0.000 30 and 0.001 80, 0.001 20 a.u., respectively. Optimization is considered complete as soon as the four conditions are simultaneously fulfilled.

DFT calculations with the PW basis set and PBE Hamiltonian were carried out by using the VASP code.[32,33] We used small core pseudopotentials for all atoms where for Sr atom $4s^2 4p^6 5s^2$ electrons are treated as valence, for Ti and O—$3s^2 3p^6 4s^2 3d^2$ and $2s^2 2p^4$, respectively. We kept a large cutoff energy of 520 eV to reduce finite sampling error and the value of 600 eV was chosen for the fast Fourier transform grid.

IV. CALCULATION OF $SrTiO_3$ AND $SrFeO_3$ BULK PROPERTIES

In this section we present some results on the bulk properties of perfect $SrTiO_3$ and $SrFeO_3$ crystals. In order to demonstrate the capabilities of the hybrid HF-DFT approach compared to the pure DFT method both in the LCAO and PW representations for $SrTiO_3$, in Table I we present the results of some bulk properties calculated by using three different approaches: the hybrid method with B3PW functional

TABLE I. Experimental and calculated lattice constant a_0, bulk modulus B, atomization energy E_{at}, and energy band gap E_{gap} of $SrTiO_3$.

	a_0 (Å)	B (GPa)	E_{at} (eV)	E_{gap} (eV)
LCAO-B3PW	3.892	193	31.4	3.6
LCAO-PBE	3.921	176	33.5	2.0
PW-PBE	3.941	172	31.7	1.8
Expt.	3.905[a]	179[b]	31.7[c]	3.3[d]

[a] Reference 39.
[b] Reference 40.
[c] Reference 41.
[d] Reference 11.

TABLE II. Experimental and calculated lattice constant a_0, bulk modulus B, and atomization energy E_{at} of ferromagnetic $SrFeO_3$.

	a_0 (Å)	B (GPa)	E_{at} (eV)
LCAO-B3PW	3.856		29.7
LCAO-PBE	3.875	168	33.0
PW-PBE	3.850	169 (171[a])	
Expt.	3.850[b]		

[a] LSDA+U calculation with VASP code from Ref. 22.
[b] Reference 42.

and two pure DFT methods in LCAO and PW basis sets with exactly the same PBE-GGA[34] Hamiltonian. The hybrid approach delivers very reasonable results both for lattice constant and for atomization energy, thus promising a good description of structural and energetic properties. The bulk modulus in the hybrid method is overestimated because the HF Hamiltonian tends to overestimate the second derivative of the energy. Also, as well known from the literature, the hybrid Hamiltonian provides the best agreement with the experimental optical band gap whereas the DFT methods underestimate this quantity considerably.[28] Note, however, that all approaches used give largely the same picture of the energy bands in the BZ as clearly seen from the calculated band structures in Fig. 1.

Table II contains the properties calculated for the case of ferromagnetic $SrFeO_3$. In this case both hybrid LCAO and DFT-PBE approaches give lattice constants very close to the experimental values. As expected the DFT-PBE method based upon PW basis expansion provides a very good description for the metallic crystal.

As to magnetic properties $SrFeO_3$ we first performed a comparative analysis of collinear ferromagnetic (FM) and antiferromagnetic (A-, C-, and G-type) states. The determined sequence of stability obtained from B3PW calculation is FM < AFM-A < AFM-C < AFM-G, i.e., the ferromagnetic state is the most favorable. These results agree with the experimental indication that the ferromagnetic interactions in $SrFeO_3$ are significantly stronger than antiferromagnetic interactions.[22] Then, for the ferromagnetic phase we considered states with different possible total spin projections and estimated the energetic sequence of spin states. From Table III we can see that all methods yield the state with $S=2$ as the most favorable one.

The calculated band structure and density of electronic states of $SrFeO_3$ in the B3PW approach are discussed in more detail in Sec. VI and shown below in Fig. 3(d). The main features of energy bands as well as the metallic nature of the crystal are compatibly well with the results of the local spin density functional approximation (LSDA) in the full-potential linearized-augmented-plane-wave approach.[25]

V. CALCULATION OF JAHN-TELLER DISTORTION IN $SrFe_xTi_{1-x}O_3$

It has been already mentioned above that in Ref. 7 a strong indication of the presence of a Jahn-Teller distortion around the Fe^{4+} impurity in $SrFe_xTi_{1-x}O_3$ has been found. A nonthermal broadening in the Fe–O bond length distribution

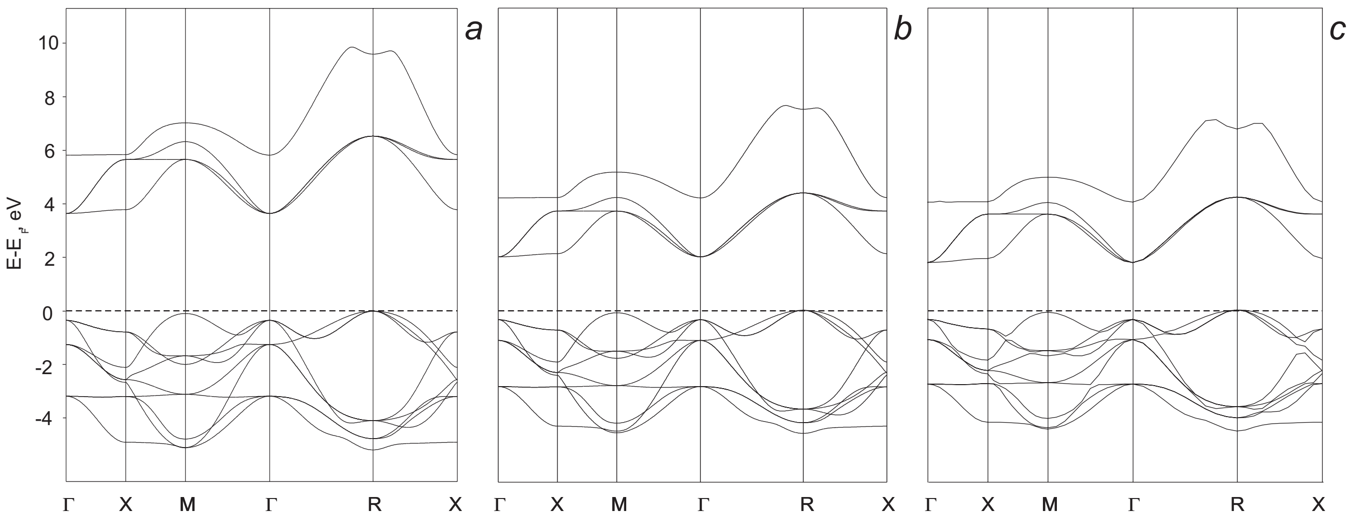

FIG. 1. Energy bands calculated by three methods: the hybrid HF-DFT with B3PW functional in LCAO (a), the DFT-PBE in LCAO (b), and DFT-PBE in PW (c). All bands are shifted at the value of Fermi energy; the dashed lines denote the top of the valence band.

TABLE III. Energy differences in eV between different magnetic spin states of ferromagnetic $SrFeO_3$ with respect to the state with $S=2$.

	$S=0$	$S=1$	$S=2$	$S=3$
LCAO-B3PW	3.2	1.6	0.0	1.3
LCAO-PBE	1.3	0.6	0.0	2.2
PW-PBE	1.0	0.4	0.0	1.8

has been determined which corresponds to a splitting of the bond lengths Δr by about 0.16 Å for the dilute system ($x \to 0$). According to the used approach the static disorder component of mean square relative displacement MSRD_{stat} is related to the bond length distribution Δr as follows:

$$\sqrt{\mathrm{MSRD}_{stat}} = \sqrt{\frac{m(r_m - r_0)^2 + n(r_n - r_0)^2}{m+n}} = \frac{\sqrt{mn}}{m+n}|\Delta r|, \tag{3}$$

being about 0.006 Å^2 for $x \to 0$. The defined above MSRD_{stat} is linked to the standard deviation for changing lengths of chemical bonds and can be used for the comparison between theoretical and experimental results.

In addition, vibrational spectroscopy permitted the study of phonon modes in the system for different iron concentrations and temperatures. The hallmark of the measured Raman spectra is a pronounced peak at 690 cm^{-1}. Its position depends only very slightly upon the iron content whereas the intensity increases from $x=0.003$ up to a maximum at $x=0.03$ and then decreases. It has been supposed[7] that this characteristic peak is caused by a vibration localized around the Fe^{4+} ion. Based on the MSRD estimates from the EXAFS experiment and on the fact that the Raman peak area decreases with increasing iron content the authors concluded that the Jahn-Teller distortion decreases for high iron concentrations as well.

To corroborate these experimental findings we performed first-principles calculation of the Jahn-Teller effect for the whole range of iron content starting from pure $SrTiO_3$ and ending at pure $SrFeO_3$ by taking several characteristic iron concentrations in between.

In the previous Hartree-Fock study[8] of Fe-doped $SrTiO_3$ it has been shown that at least a 160-atom supercell is needed to model isolated iron impurities in the material. In Ref. 27 only 40- and 80-atom supercells have been studied. Here we do not restrict ourselves to isolated iron defects but go beyond this dilute regime toward higher iron contents. In order to inspect the tendency of how the total magnitude of the distortion changes for different iron contents, we considered 80-, 135-, 160-, and 270-atom supercells in which the titanium atom in the origin is substituted by iron corresponding to 6.25%, 3.70%, 3.125%, and 1.85% iron concentrations, respectively. In the case of 50% iron content we considered two alternative iron configurations with 10-atom and 40-atom supercells.

First of all, we optimized the lattice constant of the cubic $SrTiO_3$ cell (see Table I) which was then used in our simulations of the defective system. It has been demonstrated experimentally[7] that the deviation of lattice constant in $SrFe_xTi_{1-x}O_3$ from that of pure $SrTiO_3$ is rather small for low iron content. Due to this fact, for the small iron concentrations we performed relaxation of atomic positions with fixed volume using the preliminarily optimized lattice parameter $a=3.892$ Å for pure $SrTiO_3$ whereas the Jahn-Teller distortion for 50% iron was calculated with the reoptimized lattice constant of 3.874 Å.

We carried out full optimization of atomic positions for all supercells chosen. The oxygen displacements found in the first shell of the iron defect clearly indicate that Jahn-Teller distortion takes place according to the D_{4h} point symmetry. In Table IV we summarize the information on the supercells used and the results for the distorted first oxygen shell around the Fe^{4+} impurity. The results correspond to the optimization using $2\times2\times2$ **k** mesh for all supercells except 50% contents where the denser meshes were employed. The magnitude of the total distortion $\Delta r=0.16$ Å estimated from the EXAFS experiment[7] for the dilute limit is comparable with the sum of the elongation of the Fe-O bond along the x or y axis and the contraction along the z axis (see Fig. 2). For 50% of iron content we considered one additional 40-atom supercell with four iron atoms in which defects are arranged

TABLE IV. The displacements of oxygen atoms in the first shell of the iron impurity for different iron concentrations. Inward relaxation means displacement toward the iron center. 40-atom supercell with four iron atoms in the cell simulates the orthogonal -Fe-O-Fe- chains while other supercells correspond to the distributions of isolated iron atoms (see the text for explanation). $d_{\text{Fe-Fe}}$ denotes the distance between the closest isolated iron defects.

Supercell	Extension	Iron content (%)	$d_{\text{Fe-Fe}}$ (Å)	Oxygen displacements (Å) Inward	Outward	MSRD_{stat} ($\times10^{-3}$ Å^2)
40-atom	$2\times2\times2$	50.0				2.60
10-atom	$\sqrt{2}\times\sqrt{2}\times\sqrt{2}$	50.0	5.48	0.0489	0.0665	2.96
80-atom	$2\sqrt{2}\times2\sqrt{2}\times2\sqrt{2}$	6.25	11.01	0.0545	0.0681	3.34
135-atom	$3\times3\times3$	3.70	11.68	0.0580	0.0660	3.42
160-atom	$2\sqrt{3}\times2\sqrt{3}\times2\sqrt{3}$	3.125	13.48	0.0570	0.0690	3.53
270-atom	$3\sqrt{2}\times3\sqrt{2}\times3\sqrt{2}$	1.85	16.51	0.0495	0.0795	3.70[a]

[a] The estimate of MSRD_{stat} from EXAFS experiment (Ref. 7) extrapolated to the dilute limit yields 0.006 Å^2.

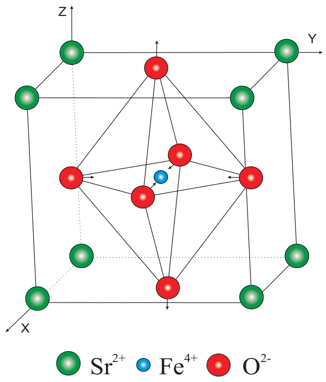

FIG. 2. (Color) Schematic view of the relaxation of six nearest oxygen atoms around Fe impurity. Four oxygen atoms in the *xy* plane relax inward whereas two atoms along the *z* axis displace outward the impurity.

in orthogonal -Fe-O-Fe- chains instead of being isolated as in all other cases. In this case the displacements of oxygen atoms exhibit a more complex pattern. While three of four iron atoms in the supercell have four shortened and two elongated Fe–O bonds, the distortion is inverted for the last fourth iron (four elongated and two shortened bonds). In order to compare theory and experiment, we calculated MSRD_{stat} for the whole range of iron concentration according to Eq. (3). From the last column of Table IV one can see that MSRD_{stat} increases with lowering the iron content giving the correct tendency of MSRD_{stat} change, known from EXAFS data, and approaching the experimental estimation for the dilute limit.

TABLE V. Energy differences in eV between different magnetic spin states in 80-atom supercell after relaxation with respect to the state with $S=2$ and energy difference ΔE between unrelaxed and relaxed supercell for $S=2$.

	$S=0$	$S=1$	$S=2$	$S=3$	ΔE
LCAO-B3PW	6.2	3.5	0.0	2.2	0.40
PW-PBE	0.9	0.4	0.0	1.5	0.46

We also checked the possibility for JT distortion in pure $\mathrm{SrFeO_3}$ in our hybrid HF-DFT computational scheme by performing a full structure optimization starting from the distorted system. The converged geometry has been very close to the perfect cubic structure indicating that JT distortion is unfavorable. This result is consistent with the experimentally

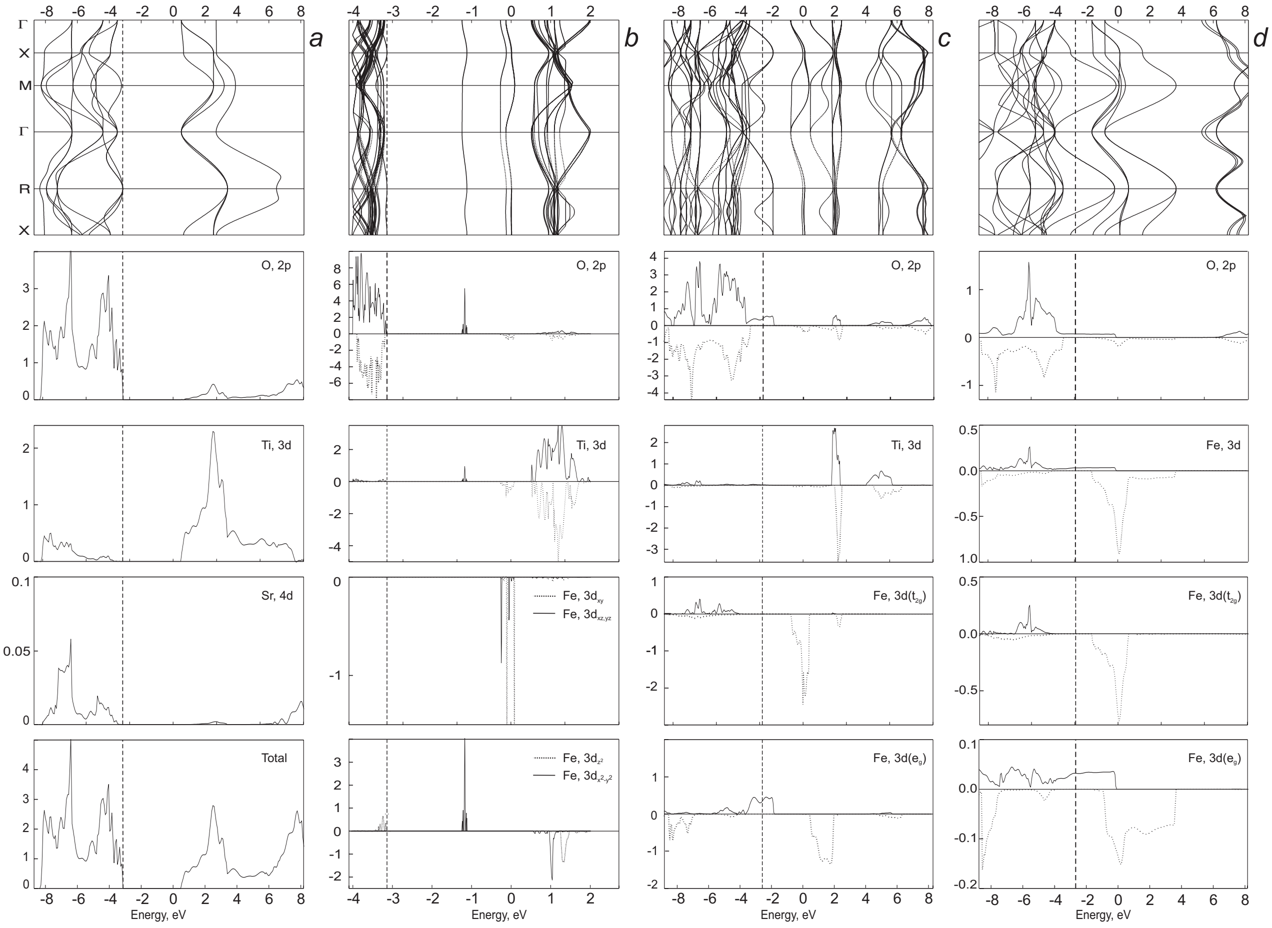

FIG. 3. Calculated band structures and projected density of electronic states (PDOS) for (a) $\mathrm{SrTiO_3}$, (b) $\mathrm{SrFe_{0.0625}Ti_{0.9375}O_3}$, (c) $\mathrm{SrFe_{0.5}Ti_{0.5}O_3}$, and (d) $\mathrm{SrFeO_3}$. The vertical dash lines denote Fermi energy level. Solid lines are applied to spin up and dot lines to spin down electrons. The values for PDOS are in arbitrary units. In all cases only the top of valence band and the bottom of conduction band are presented.

observed absence of a JT distortion in pure SrFeO$_3$.

Different spin states for the 80-atom supercell after relaxation were calculated to show that the $S=2$ state is the most favorable also for the defective system as well as for pure SrFeO$_3$ (see Table V).

In addition, we estimated the formation energy of substitutional iron defect for all iron concentrations via

$$E_{\mathrm{Fe}}^{form} = E(def) - E(\mathrm{Fe}) + E(\mathrm{Ti}) - E(per), \qquad (4)$$

where E(Fe) [−1263.360313 a.u.] and E(Ti) [−57.983605 a.u.] are the energies of iron and titanium atoms in gas phase, while $E(def)$ and $E(per)$ are those for defective and perfect crystals, respectively.

We found that the formation energy of 1.79 eV for the most dilute system under consideration is only 0.01 eV higher than in the 6.25% case. This substitution energy decreases to 1.59 eV for 50% case and to 1.57 eV for pure SrFeO$_3$.

VI. ELECTRONIC PROPERTIES OF SrFe$_x$Ti$_{1-x}$O$_3$

In this section we present the results with respect to the electronic structure of SrFe$_x$Ti$_{1-x}$O$_3$ solid solution. Figure 3 contains the calculated band structures and the projected density of electronic states (PDOS) for $x=0\%$ (a), 6.25% (b), 50% (c), and 100% (d).

Figure 3 shows also the calculated band structure and the PDOS of pure SrTiO$_3$. The top of the valence band mainly consists of O 2p states while predominantly Ti 3d states contribute to the bottom of conduction band. These facts are reflected in our calculation of the band structure and the PDOS in Fig. 3(a).

The second limiting case is SrFeO$_3$ which exhibits metallic properties without band gap as illustrated in Fig. 3(d). From the calculated magnetic moments we can conclude that the magnetization is mostly caused by the iron atom (3.79μ_B) while the magnetic moments of oxygen atoms induced by Fe–O bonding are very small (0.07μ_B). It is clearly seen from the comparison of the PDOS for spin up and spin down electron densities that the effect of spin polarization is more pronounced for Fe 3d states. The PDOS [Fig. 3(d)] also indicates that a strong mixing between Fe 3d and O 2p takes place near the Fermi level. Furthermore, the major contribution in the vicinity of the Fermi level originates from the e_g states of iron and the O 2p states. These main features of the electronic and magnetic properties of ferromagnetic SrFeO$_3$ agree well with a cluster model (CI) prediction[15] and a recent LSDA simulation in the PW basis set.[22]

To study the change of the electronic structure between these two limiting cases of $x=0$ and $x=1$ we also calculated the energy bands and PDOS for two levels of iron doping in SrTiO$_3$, namely, 6.25% and 50% iron [Figs. 3(b) and 3(c)]. For 6.25% (as in the case of pure SrTiO$_3$) the top of the valence band is mainly formed by O 2p orbitals, and the bottom of virtual bands predominantly consists of Ti 3d states. However, there is a noticeable contribution of Fe 3d_{z^2} and 3$d_{x^2-y^2}$ to the valence band in the pre-Fermi energy region. The spin down electron densities of Fe 3d states form narrow sharp bands which are combined into broader peaks in the case of 50% iron (panel c). We can also notice that when going to 50% iron the Fermi level is moving to slightly higher energy, and that 3d_{z^2} and 3$d_{x^2-y^2}$ energy bands are merging in the Fermi energy region. These bands are further broadening when the iron content is increased while the Fermi energy is nearly the same in the 50%-doped system and in pure SrFeO$_3$. The same applies to the O 2p states when going from 6.25% iron via 50% to pure SrFeO$_3$. It is also seen that the Ti 3d orbitals, still dominating in the bottom of the conducting band for the 6.25% of iron, split into two subbands and decrease in the 50% case.

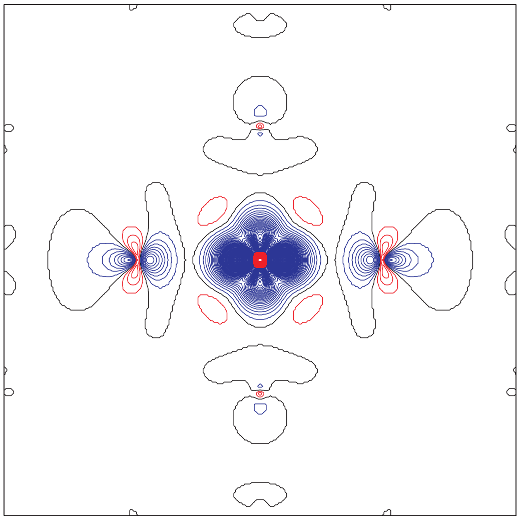

FIG. 4. (Color) Two-dimensional difference electron density map projected onto the (010) plane for 80-atom supercell containing iron defect and nearest ions. Black, red, and blue solid isolines correspond to the zero, negative, and positive values of electron density, respectively. Isodensity curves are drawn from −1.0 to 1.0 e Å^{-3} with increments of 0.01 e Å^{-3}.

In Fig. 4 the difference electron density map for 80-atom supercell with iron impurity in the center is displayed. This density is defined as the total density difference of defective and perfect systems plus the difference between titanium and iron atoms projected onto the (010) plane. The redistribution of the electron density around the iron impurity demonstrates that iron attracts more electron density than titanium at the same site. This reflects the more ionic Ti–O bond in bulk SrTiO$_3$ compared to Fe-O bond in defective SrFe$_x$Ti$_{1-x}$O$_3$. The computed atomic magnetic moment of the iron is 3.56μ_B being slightly less than in bulk SrFeO$_3$ (3.79μ_B). These results show that the four unpaired electrons are rather localized on the iron atom in bulk SrFeO$_3$.

TABLE VI. The Mulliken effective atomic charges q in perfect SrTiO$_3$, SrFeO$_3$, and 80-atom supercell with iron impurity. M denotes Ti or Fe atom in bulk crystals and Fe atom in the supercell.

	$q(M)$	q(O)	
SrTiO$_3$	2.36	−1.41	
SrFeO$_3$	2.26	−1.38	
SrFe$_{0.0625}$Ti$_{0.9375}$O$_3$	2.28	−1.39(O$_{x,y}$)	−1.43 (O$_z$)

In Table VI the calculated Mulliken effective charges on atoms are listed. It is seen that the iron charge in $SrFeO_3$ is slightly less than the titanium charge in $SrTiO_3$ correctly reflecting the slightly larger covalent character of $SrFeO_3$ bulk crystal. However, it is known that in some cases the traditional Mulliken population analysis can fail and other approaches must be applied as demonstrated, e.g., for the example of the more ionic $SrZrO_3$.[43]

VII. CONCLUSIONS

The present calculations have demonstrated that the hybrid HF-DFT LCAO method with B3PW exchange-correlation functional allows one to quantitatively describe the Jahn-Teller distortion in $SrFe_xTi_{1-x}O_3$ solid solution. The calculation of the Jahn-Teller distortion around the Fe^{4+} impurities for different iron concentrations (50%, 6.25%, 3.70%, 3.125%, and 1.85%) show that the distortion is the largest for very dilute iron content, less pronounced for 50% of iron, and absent in the case of pure $SrFeO_3$. These results agree with the experimental observation whereas the computed magnitude of the Jahn-Teller distortion for dilute system is well comparable with recent experimental estimates from EXAFS data. The electronic structure calculations indicate that $SrFe_xTi_{1-x}O_3$ with more than 50% iron is metallic, and that its conductivity is caused by a strong mixing of O $2p$ and Fe $3d$ (e_g) states in the pre-Fermi region.

ACKNOWLEDGMENTS

The authors gratefully thank E. A. Kotomin, R. Merkle, and A. Kuzmin for many fruitful and stimulating discussions. R. Merkle is particularly acknowledged for critically reading the manuscript.

---

*v.alexandrov@fkf.mpg.de

[1] Per G. Sundell, M. E. Björketun, and G. Wahnström, Phys. Rev. B **73**, 104112 (2006).

[2] A. Kuwabara and I. Tanaka, J. Phys. Chem. **108**, 9168 (2004).

[3] H. Meštrić, Rüdiger-A. Eichel, K.-P. Dinse, A. Ozarowski, J. van Tol, L. C. Brunel, H. Kungl, M. J. Hoffmann, K. A. Schönau, M. Knapp, and H. Fuess, Phys. Rev. B **73**, 184105 (2006).

[4] R. A. De Souza, J. Fleig, R. Merkle, and J. Maier, Z. Metallkd. **94**, 218 (2003).

[5] S. Rodewald, J. Fleig, and J. Maier, J. Am. Ceram. Soc. **84**, 521 (2001).

[6] R. Merkle and J. Maier, Angew. Chem., Int. Ed.(to be published).

[7] M. Vračar, A. Kuzmin, R. Merkle, J. Purans, E. A. Kotomin, J. Maier, and O. Mathon, Phys. Rev. B **76**, 174107 (2007).

[8] R. A. Evarestov, S. Piskunov, E. A. Kotomin, and G. Borstel, Phys. Rev. B **67**, 064101 (2003).

[9] M. Vaccari and P. Fornasini, J. Synchrotron Radiat. **13**, 321 (2006).

[10] A. D. Becke, J. Chem. Phys. **98**, 5648 (1993).

[11] K. van Benthem, C. Elsasser, and R. H. French, J. Appl. Phys. **90**, 6156 (2001).

[12] J. B. MacChesney, P. K. Gallagher, and D. N. E. Buchanan, J. Chem. Phys. **43**, 1907 (1965).

[13] J. Zaanen, C. Westra, and G. A. Sawatzky, Phys. Rev. B **33**, 8060 (1986).

[14] A. E. Bocquet, A. Fujimori, T. Mizokawa, T. Saitoh, H. Namatame, S. Suga, N. Kimizuka, Y. Takeda, and M. Takano, Phys. Rev. B **45**, 1561 (1992).

[15] M. Abbate, G. Zampieri, J. Okamoto, A. Fujimori, S. Kawasaki, and M. Takano, Phys. Rev. B **65**, 165120 (2002).

[16] S. Piskunov, E. Heifets, R. I. Eglitis, and G. Borstel, Comput. Mater. Sci. **29**, 165 (2004).

[17] D. E. Usvyat, R. A. Evarestov, and V. P. Smirnov, Int. J. Quantum Chem. **100**, 352 (2004).

[18] W. Zhong, R. D. King-Smith, and D. Vanderbilt, Phys. Rev. Lett. **72**, 3618 (1994).

[19] S. Tinte, M. G. Stachiotti, C. O. Rodriguez, D. L. Novikov, and N. E. Christensen, Phys. Rev. B **58**, 11959 (1998).

[20] S. Mathi Jaya, R. Jagadish, R. S. Rao, and R. S. Asokamani, Phys. Rev. B **43**, 13274 (1991).

[21] S. Matar, Prog. Solid State Chem. **31**, 239 (2003).

[22] I. R. Shein, K. I. Shein, V. L. Kozhevnikov, and A. L. Ivanovskii, Phys. Solid State **47**, 2082 (2005).

[23] D. E. Ellis and G. S. Painter, Phys. Rev. B **2**, 2887 (1970).

[24] E. I. Yurieva, V. L. Kozhevnikov, and A. L. Ivanovskii, J. Struct. Chem. **47**, 553 (2006).

[25] I. R. Shein, V. L. Kozhevnikov, and A. L. Ivanovskii, JETP Lett. **82**, 220 (2005).

[26] I. B. Bersuker, *The Jahn-Teller Effect* (Cambridge University Press, Cambridge, 2006).

[27] Z. Chao, W. Chun-Lei, Li Ji-Chao, and Y. Kun, Chin. Phys. **16**, 1422 (2007).

[28] R. A. Evarestov, *Quantum Chemistry of Solids: The LCAO First Principles Treatment of Crystals*, Springer Series in Solid-State Science Vol. 153 (Springer, Berlin, 2007).

[29] F. Cora, M. Alfredsson, G. Mallia, D. S. Middlemiss, W. C. Mackrodt, R. Dovesi, and R. Orlando, Struct. Bonding (Berlin) **113**, 171 (2004). Review paper is online: http://www.crystal.unito.it/tutojan2004/tutorials

[30] R. Dovesi, V. R. Saunders, C. Roetti, R. Orlando, C. M. Zicovich-Wilson, F. Pascale, B. Civalleri, K. Doll, N. M. Harrison, I. J. Bush, Ph. D'Arco, and M. Llunell, *Crystal 2006 User's Manual* (University of Turin, Turin, 2006).

[31] J. Paier, R. Hirschl, M. Marsman, and G. Kresse, J. Chem. Phys. **122**, 234102 (2005).

[32] G. Kresse and J. Furthmüller, *VASP the Guide* (University of Vienna, Austria, 2003).

[33] G. Kresse and J. Hafner, Phys. Rev. B **48**, 13115 (1993); **49**, 14251 (1994).

[34] J. P. Perdew, K. Burke, and M. Ernzerhof, Phys. Rev. Lett. **77**, 3865 (1996).

[35] P. J. Hay and W. R. Wadt, J. Chem. Phys. **82**, 270 (1984); **82**, 284 (1984); **82**, 299 (1984).

[36] M. Catti, G. Valerio, and R. Dovesi, Phys. Rev. B **51**, 7441 (1995).

[37] H. J. Monkhorst and J. D. Pack, Phys. Rev. B **13**, 5188 (1976).

[38] H. B. J. Schlegel, Comput. Chem. (Oxford) **3**, 214 (1982).

[39] Y. A. Abramov and V. G. Tsirelson, Acta Crystallogr., Sect. B: Struct. Sci. **51**, 942 (1995).

[40] *Ferroelectrics and Related Substances*, Landolt-Bornstein New Series Group III, Vol. 3, edited by K. H. Hellwege and A. M. Hellwege (Springer, Berlin, 1969).

[41] D. Ricci, G. Bano, G. Pacchioni, and F. Illas, Phys. Rev. B **68**, 224105 (2003).

[42] T. Takeda, Y. Yamaguchi, and H. Watanabe, J. Phys. Soc. Jpn. **33**, 967 (1972).

[43] R. A. Evarestov, I. I. Tupitsyn, A. V. Bandura, and V. E. Alexandrov, Int. J. Quantum Chem. **106**, 2191 (2006).